Effect of ambient pressure on laser ablation and plume expansion dynamics: A numerical simulation

Zhaoyang Chen,[a] Davide Bleiner, and Annemie Bogaerts
Department of Chemistry, University of Antwerp, Universiteitsplein 1, B-2610 Wilrijk-Antwerp, Belgium

(Received 19 August 2005; accepted 9 February 2006; published online 23 March 2006)

A comprehensive numerical model is applied to the study of the effect of ambient pressure in laser ablation, more specifically on the copper target heating, melting and vaporization, and the resulting plume expansion in the helium gas, as well as on plasma formation in the plume. Under the laser pulse condition investigated [5 ns full width at half maximum (FWHM) and 10^9 W/cm^2 peak irradiance], the calculated results show that the characteristics of the surface temperature and the evaporation depth are very similar even when the ambient pressure varies greatly. The influence of the ambient pressure on the fraction of absorbed laser energy is also small. The maximum ablated material vapor density in the plume is influenced slightly by the different pressures. Before 40 ns, the maximum plume temperature for various ambient pressures is in the order of a few 10^4 K. However, the effect of ambient pressure on the plume length is quite large. A specific calculation for a Gaussian-shaped laser pulse with 6 ns FWHM and 2.76×10^9 W/cm^2 peak irradiance is made. The calculated evaporation depth agrees well with the experimental data. Therefore, the model can be useful to predict trends in target and plume (plasma) characteristics, which are difficult to obtain experimentally for various ambient pressures. © *2006 American Institute of Physics*.
[DOI: 10.1063/1.2182078]

I. INTRODUCTION

Laser ablation (LA) is used for a growing number of applications, such as pulsed laser deposition (PLD),[1,2] nanoparticle manufacturing,[3,4] cluster production[5] for the analysis of solid materials,[6–9] etc. The study of material expanding into vacuum or in ambient background gas is an important issue in gas dynamics (see Ref. 10) and for laser ablation. Laser pulses used in PLD have typically a duration of 10–100 ns and an energy fluence of 1–10 J/cm^2 (with peak irradiance of 10^7–10^9 W/cm^2). When LA is used for solid material analysis, e.g., laser-induced breakdown spectroscopy (LIBS),[11] or LA as a sample introduction method for an inductively coupled plasma (ICP), the laser pulses have typically a laser irradiance between 10^8 and 10^9 W/cm^2 and a duration of a few nanoseconds. However, for PLD, the ambient gas pressure generally ranges from 10 to 100 Pa; but for the applications in LIBS or ICP, the background gas is typically at 1 atm.[6–9]

Laser-produced plasma is transient in nature with characteristic parameters that evolve quickly and are highly dependent on irradiation conditions such as incident laser intensity and pulse duration, laser wavelength, irradiation spot size, ambient gas composition, and ambient pressure. The plume expansion, which may be strongly influenced by the laser-induced plasma, can be investigated either by Monte Carlo (MC) simulations,[12–16] by hydrodynamic models,[3,17–27] or by a hybrid model (combination of both).[28,29] It should be emphasized that it would take much longer calculation time to study the plume expansion into a high-pressure background gas with the MC simulations or hybrid models. Therefore generally one makes use of hydrodynamic models to study the plume expansion into ambient gas at higher pressure. It is well known that, compared to the expansion into vacuum, the interaction of the plume with an ambient gas is a far more complex gas dynamic process due to the occurrence of several physical processes involved, such as deceleration, attenuation, thermalization of the ablated species, diffusion, recombination, and formation of shock waves.[30] In the study of the plume expansion into a background gas, mostly hydrodynamic models have been used to treat the ambient pressures limited till maximum about 100 Pa.[18,21–24] The plume expansion into 1 atm background gas was numerically investigated in Refs. 3, 17, 19, 26, 31, and 32. The general effect of the background gas is reported to be the spatial confinement and slowing down of the expanding plume. Moreover, the material can even move backward.[3,33] Among the modeling works for low- and high-pressure ambient gases mentioned above, some authors have not considered the ionization of ablated material at all; on the other hand, some authors have simply neglected the very important interaction between laser and vapor (plasma) although they have taken into account the effects of mass and forced diffusion and thermal conduction and viscosity by the use of three-dimensional axisymmetric compressible Navier-Stokes equations.[21,27]

In our previous work, a model was developed to consider the ionization of both ablated material and ambient gas during the early stage of plume expansion.[31,32] Such a modeling is, however, very important for the various applications mentioned above, where the laser irradiance is around 10^8–10^9 W/cm^2 and where evaporation takes place in 1 atm nonreactive background gas. Especially, Ref. 32 investigated systematically the effect of laser parameters on the laser ab-

[a]Electronic mail: zhaoyang.chen@ua.ac.be

lation of Cu and plume expansion into 1 atm He background gas. Basically, the model is developed for nanosecond UV excimer or visible laser pulses, metal targets such as Cu or Al, and nonreactive ambient gas such as He or Ar. If chemical reactions between the target element and the ambient gas take place, the model will fail. The irradiance ranges from 10^8 to 10^9 W/cm^2, which is typically used for laser ablation as a sample introduction method for ICP spectrometry. It can, however, also be of interest to other applications, which work under similar conditions. In the present work, we will apply this model to study the effect of various pressures of ambient gas (He) on laser ablation of Cu and plasma formation at the early stage (i.e., until 40 ns) as well as plume expansion into ambient He gas. We will also compare the calculated results with an experimental result and show the good agreement on the evaporation depth.

It should be pointed out that the validity of the planar expansion of the plume in the early stage depends highly on the pressure of ambient gas and the laser spot radius. Sharma and Thareja observed that at times above 60 ns the plume expansion is conical at pressures of 0.1 Torr or less, whereas at pressures of 1 Torr and above the expansion is spherical.[34] Besides, at the later stages of the plume or plasma expansion, the assumption of local thermodynamic equilibrium is no longer valid because three-body recombination comes into play, which means that the Saha equation is not valid anymore. Thus, we restrict our calculations up till 40 ns, so that for all applied ambient pressures the planar expansion of the plume is a fairly good approximation and the Saha equation is still valid. On the other hand, the plume splitting[4] and Rayleigh-Taylor instability[34] are not considered in the paper because they do not occur in the early stage (less than 40 ns). Moreover, under the condition of the applied laser with a pulse width of 5 ns of full width at half maximum (FWHM) the laser pulse is finished at around 14 ns, hence 40 ns is a long enough period of time for the study of the material ablation rate and the laser-plasma interaction and the early stage of plume expansion. Finally, it is worth mentioning that the present paper focuses exactly on this early stage, because it is most difficult to model, especially in the presence of an ambient gas, due to the strong laser-plume interaction and intense plasma formation, but this early stage is very important for determining further the plume expansion dynamics.

II. DESCRIPTION OF THE MODEL

The model for laser ablation of a Cu target in 1 atm He gas was explained in detail in Ref. 31. In this paper, although the ambient pressure is varied, the principle and the procedure of the model are the same as that for 1 atm. Hence, in the present paper we will not formulate the equations again, but we will only briefly summarize qualitatively the various processes which are described in the model.

The heating of the Cu target, as a result of laser-solid interaction, is described with a heat conduction equation, which yields the temperature distribution inside the target, as a function of time. When the temperature rises above 1358 K (i.e., the melting point of Cu), the Cu target starts melting and the same heat conduction equation is used for the molten phase, but using the appropriate thermal data for liquid Cu. When the temperature rises further, vaporization can become significant and the vaporization pressure is calculated from the surface temperature, by integrating the Clausius-Clapeyron equation. The vapor pressure yields the vapor density at the surface and this is used as an input (i.e., boundary condition) in the second part of the model, together with the vapor velocity and temperature at the surface. The expansion of the evaporated Cu material into He background gas is described with one-dimensional (1D) Navier-Stokes equations, for conservation of total mass density, vapor mass density, momentum, and energy, in a binary gas mixture. Naturally, when the plume expansion into vacuum is considered, the 1D Navier-Stokes equations are simplified to 1D Euler equations which were described and discussed already in a previous work (e.g., see Ref. 35). Generally speaking, the set of 1D Navier-Stokes equations is much more complicated than the corresponding set of equations for expansion in vacuum,[35] because it contains gas mixing terms, i.e., thermal conductivity, viscosity, and diffusion. Hence, it appeared to be much more difficult to solve these equations. A more detailed explanation, also with respect to the appropriate use of boundary conditions, is given in Ref. 31. Because of the high temperature in the expanding plume, a plasma is created, resulting in the formation of electrons and ions of the Cu vapor and He gas. For the typical conditions of LA and LIBS, the temperature can be so high that beside Cu^+ ions Cu^{2+} ions are also formed. The first-order and second-order ionizations of Cu and the first-order ionization of He are calculated with the Saha-Eggert equations, because the plasma is considered to be in local thermal equilibrium. From the calculated fraction of Cu^+, Cu^{2+}, Cu^0, He^+, He^0, and electrons, in combination with the calculated densities of Cu vapor and He background gas, the densities of these species are computed. Finally, because of the formation of a plasma in front of the target, the laser beam will be partially absorbed before it reaches the target, i.e., so-called "plasma shielding." The three dominant absorption mechanisms are electron-ion and electron-neutral inverse bremsstrahlung and photoionization of excited atoms. The formulas for the absorption coefficients of these processes are presented in Ref. 31. Based on these absorption coefficients, the laser irradiance reaching the target, i.e., after plasma shielding, is calculated. The different parts of the model are strongly coupled, because the target evaporation determines the plume expansion and the plume affects the target as well. Hence, the boundary condition for the target part has to be obtained from the plume part, and vice versa.[31] Moreover, the absorption of the laser beam in the plasma affects the laser-solid interaction, because the laser energy reaching the target can be considerably attenuated, and it also influences the plume temperature (i.e., gain and loss terms in the energy conservation equation). Therefore, the various parts of the model need to be solved simultaneously as a function of time, in order to obtain an overall picture of the laser-solid interaction, followed by plume expansion and plasma formation. More quantitative details about the complete model can be found in Ref. 31.

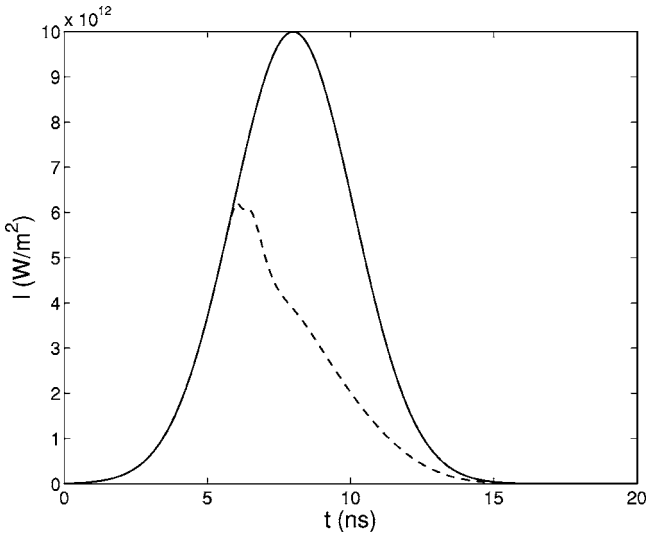

FIG. 1. Laser intensity-time profile assumed in the model. It is a Gaussian-shaped pulse with 5 ns full width at half maximum and peak irradiance of 1×10^9 W/cm^2. The solid line represents the original laser pulse and the dashed line represents the calculated laser irradiance arriving at the target, after passing through the plume (plasma).

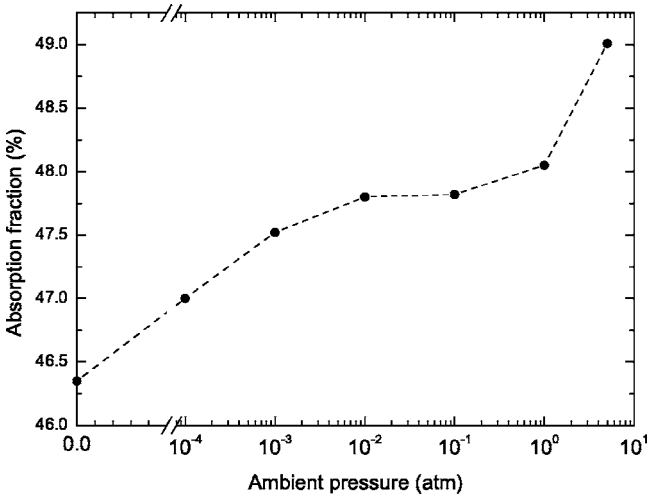

FIG. 2. Calculated fraction of laser energy absorbed by the plume as a function of ambient pressure. The original laser pulse is given in Fig. 1.

III. NUMERICAL RESULTS AND DISCUSSIONS

The calculations are performed for a Gaussian-shaped laser pulse with a wavelength of 266 nm, full width at half maximum of 5 ns, and peak laser irradiance of 10^9 W/cm^2 (see Fig. 1, solid line). Integrated over the entire pulse, this yields a fluence of 5.32 J/cm^2. In the calculations, we follow only one laser pulse. The ambient gas is He and its pressure varies from 0 to 5 atm. In the following the results for various ambient pressures at 0, 10^{-4}, 10^{-3}, 10^{-2}, 10^{-1}, 1, and 5 atm will be presented and compared.

The dashed line in Fig. 1 shows the laser irradiance arriving at the target, after passing through the plume when the ablation of Cu occurs in vacuum. One can see that a large fraction of laser energy is absorbed by the plume. Comparing the shape of absorption line with that in Refs. 35 and 36, one may find that the result is rather different from the previous ones. The main reason is that in the present paper the calculation of ionization degree in the first cell in the plume is improved. In Refs. 35 and 36, the ionization degree in the first cell was determined by the target surface temperature through the Langmuir-Saha equation. In the present work, the target surface temperature and the Langmuir-Saha equation are only applied at the left interface of the first cell, which is more reasonable than before. The ionization degree in the first cell in the plume is still determined by the Saha-Eggert equations like in other cells.

The laser absorption at other ambient pressures is not shown here, since the absorption line shapes for ambient pressures ranging from 0 to 5 atm are very similar to the dashed line shown in Fig. 1 except that the absorption fractions differ slightly. Comparing the calculated laser absorption with the experimental measurements of transient evolution of the transmitted power with a Cu target during excimer laser ablation in air at 1 atm pressure,[37] one can conclude that the current improvement in the calculation of ionization degree in the first cell is necessary and is able to predict accurately the laser irradiance arriving at the target surface.

Figure 2 presents the laser absorption fraction occurring at various ambient pressures with the same laser condition (i.e., a Gaussian laser pulse with 5 ns FWHM and 10^9 W/cm^2 peak irradiance). One can see that the absorption fraction increases monotonously with the ambient pressure. However, it is observed in Fig. 2 that the absorption fraction only changes from 46.4% for the case of vacuum to 49.0% for the case of ambient He gas at 5 atm pressure. The result suggests that there is a very similar plasma feature in the plume expansion at the early stage with the same target and laser pulse for various ambient pressures. It should be pointed out that this may be true only when there is no chemical reaction between the ablated material and the ambient gas. If chemical reactions take place, the effect of ambient pressure on the laser-induced plasma must be significant.

Furthermore, the similar laser absorption behavior at various ambient pressures can lead to a similar process of heating, melting, and vaporization in the target as a result of more or less the same laser energy deposition on the target. The calculated maximum target surface temperature for different ambient pressures is plotted in Fig. 3. The maximum surface temperature for different ambient pressures changes from 7025 to 7290 K when the ambient pressure changes from 0 to 5 atm. One can see that the trend of the maximum surface temperature along with the ambient pressure is just opposite from that of the absorption fraction, as is expected, since the larger absorption by the plasma leads to a smaller laser energy deposited on the target. Thus, one can expect that the maximum evaporation rate of target for different ambient pressures should change accordingly. This is shown in Fig. 4. Under the same laser condition, the maximum evaporation rate is about 11.37 m/s for the vacuum case and it drops to 9.6 m/s when the ambient pressure equals 5 atm. However, when the ambient pressures range from 0.01 to 1 atm, the maximum evaporation rate changes very little.

Figure 5 presents the calculated evaporation depth at

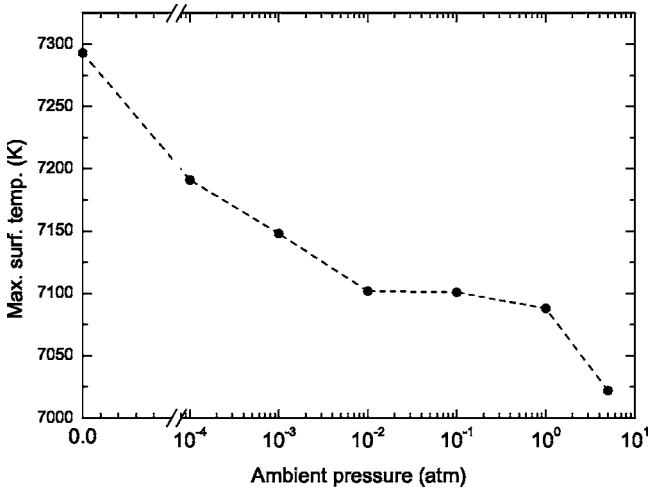

FIG. 3. Calculated maximum surface temperature as a function of ambient pressure for the condition shown in Fig. 1.

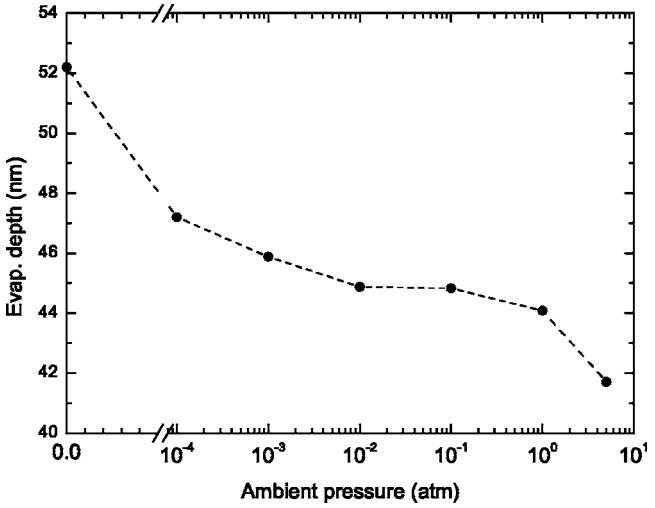

FIG. 5. Calculated evaporation depth as a function of ambient pressure for the condition shown in Fig. 1.

20 ns for different ambient pressures. It appears that the target material is ablated more efficiently in vacuum than in ambient gas. This prediction somehow contradicts with the experimental observation of excimer laser ablation of thin gold films on a quartz crystal microbalance at various argon background pressures reported by Zhang *et al.*[38] Notice that in their experiments the applied laser fluence is very low (less than 1.8 J/cm^2) and the laser-induced plasma may not be formed. In our case, the ambient pressure dependence of evaporation depth is mainly attributed to the plasma shielding. However, to clarify the validity of our model, a comparison between the simulation and experimental measurements will be given at the end of this section.

The plume expansions into vacuum and into 1 atm background gas were presented before (e.g., see Refs. 31 and 35 and references therein). Here we shall show the results for the ambient pressure at 0.1 atm. Figure 6 shows the calculated Cu vapor and background gas number densities at different times. One can see that, at an early stage of the ablation, for example, at 8 ns, the Cu vapor density is highest at the target (almost 2×10^{26} m^{-3}) and it drops gradually as a function of distance away from the target surface in the plume and very rapidly at the plume front. When time evolves, the situation has changed, i.e., the Cu vapor density tends to vary less severely as a function of position in the plume. When the time evolves further, the plume size increases. Accordingly, the maximum value of Cu vapor den-

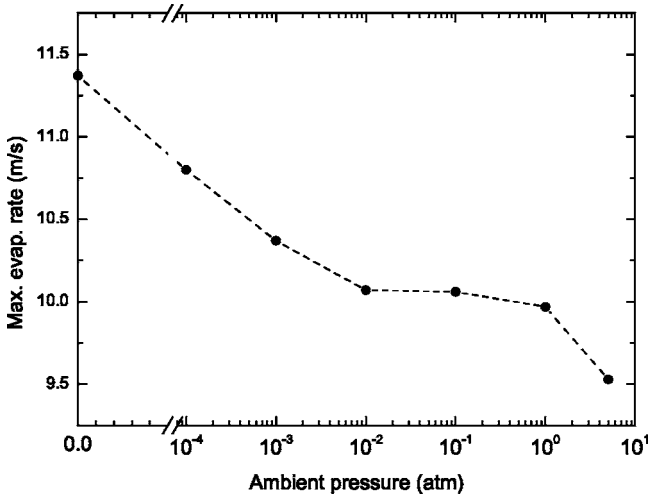

FIG. 4. Calculated maximum evaporation rate as a function of ambient pressure for the condition shown in Fig. 1.

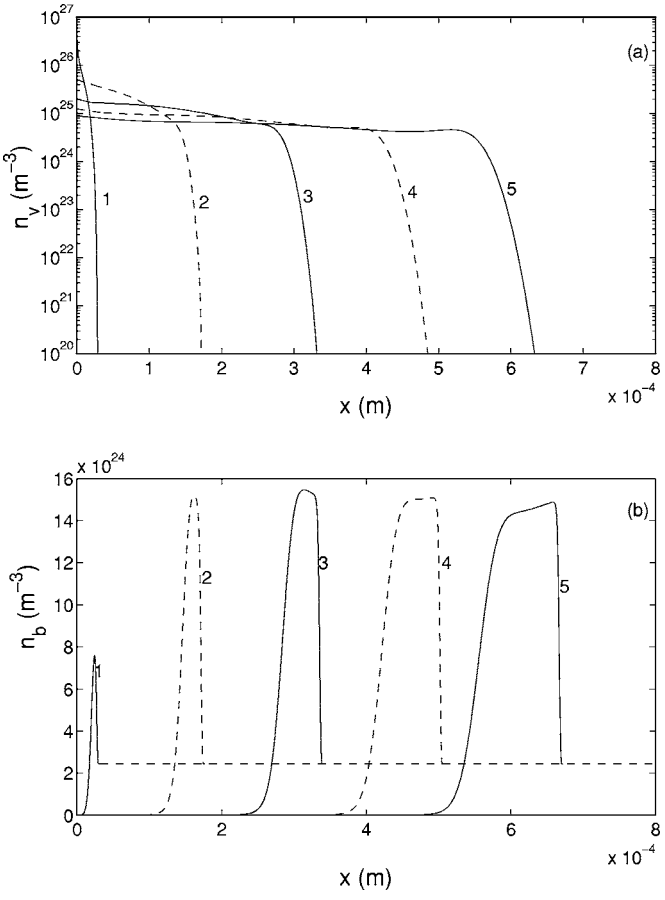

FIG. 6. Spatial distribution of (a) calculated Cu vapor density and (b) calculated ambient He gas density, at different times: 8 (1), 16 (2), 24 (3), 32 (4), and 40 ns (5), for the laser condition shown in Fig. 1 and ambient pressure at 0.1 atm.

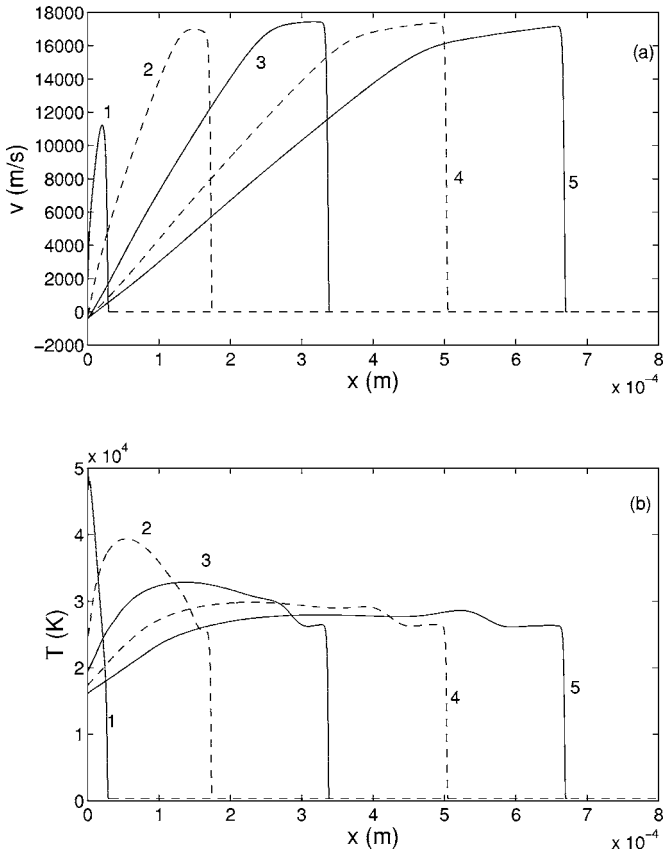

FIG. 7. Spatial distribution of (a) calculated plume velocity and (b) calculated plume temperature, at different times: 8 (1), 16 (2), 24 (3), 32 (4), and 40 ns (5), for the laser condition shown in Fig. 1 and ambient pressure at 0.1 atm.

sity decreases along with time since the vapor expands into a bigger space but there is no material supply after the evaporation process stops. Meanwhile, in Fig. 6(b) one can see that the background gas He is gradually pushed away by the Cu vapor, forming a compression shock wave. The highest value of He number density n_b can be as large as 1.55×10^{25} m^{-3} at 24 ns. Note that the value of He number density corresponding to 0.1 atm at room temperature is only 2.45×10^{24} m^{-3}. According to the so-called Sedov shock-wave theory (e.g., see Ref. 39), the ratio of the number density just at the shock front to that in the undisturbed region is $(\gamma+1)/(\gamma-1)$. When $\gamma=5/3$, this ratio equals 4. Our calculated number density ratio during the laser pulse-on period is about 5, which is somewhat larger than the predicted value of 4. This is because there is always extra material and energy added to the plume during the pulse-on period, which is not accounted for in the Sedov shock-wave theory. When the pulse has passed, the number density ratio will gradually drop to the ideal value of 4.

Figure 7(a) presents the plume velocity distribution at different times. The plume expansion into 0.1 atm background gas is expected to be slower than expansion into vacuum. When the laser pulse is finished (at approximately 16 ns), the maximum velocity is around 17 000 m/s. At 32 ns, the velocity of the shock wave reaches 17 500 m/s. Comparing the expansion into vacuum, where the plume velocity was typically calculated to be around

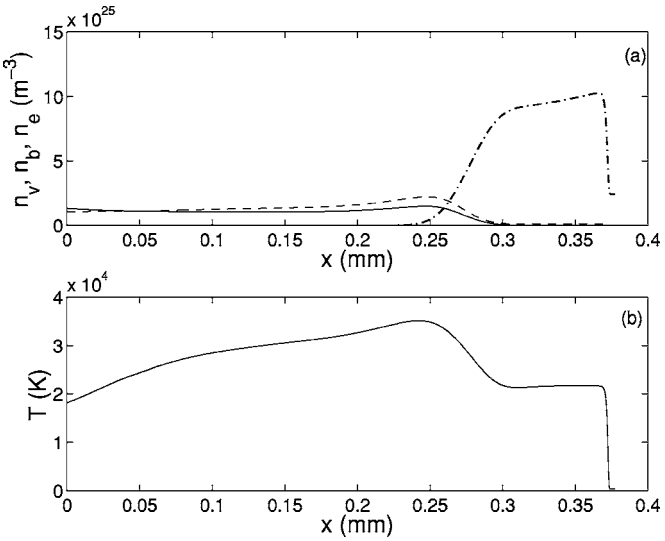

FIG. 8. Spatial distribution of (a) calculated Cu vapor density (solid line), calculated ambient gas density (dash-dotted line), and calculated electron density (dashed line) and (b) calculated plume temperature at 30 ns, for the laser condition shown in Fig. 1 and ambient pressure at 1 atm.

20 000–30 000 m/s,[35] shows that the existence of the background gas greatly reduces the plume velocity and thus the plume expansion is confined to a smaller region. On the other hand, the plume expansion with the presence of ionization is faster than that without ionization. This can be seen from Ref. 26, in which the maximum plume velocity is only about 3000 m/s, although similar conditions were applied.

The temperature distribution in the plume is presented in Fig. 7(b). Under the laser condition applied in the paper, ionization is observed to occur after 6 ns and thermionic emission and photoionization of Cu may play major roles to start the ionization process. Subsequently, the plume can absorb energy directly from the laser beam due to inverse bremsstrahlung (IB) and photoionization (PI) processes, which causes the plume temperature to increase further, resulting in fast ionization of the plume. At 8 ns, the maximum temperature in the plume appears nearby the target surface. At a later time, the peak of temperature is shifted to the center part of the plume and its value can be higher than that at the shock-wave front. This behavior is quite different from that reported in Ref. 26. This is because if there is no ionization, the maximum temperature always locates at the front of the shock wave. However, because of laser absorption in the plume due to the existence of electrons and ions, the center part of the plasma may have a higher temperature than the shock-wave front. After the laser extinguishes (around 16 ns), the temperature of the plasma drops gradually. This is because the plasma drives the shock wave moving forward to push the ambient gas away and releases some energy into the environment by bremsstrahlung radiation.

In order to have a global viewpoint of plume expansion at various ambient pressures, we want to present plume length, maximum vapor density, maximum plume temperature, and maximum electron number density at different times for various ambient pressures. Before doing so, some different characteristics of the plume for high and low pressures should be clarified first. Figure 8 shows the spatial

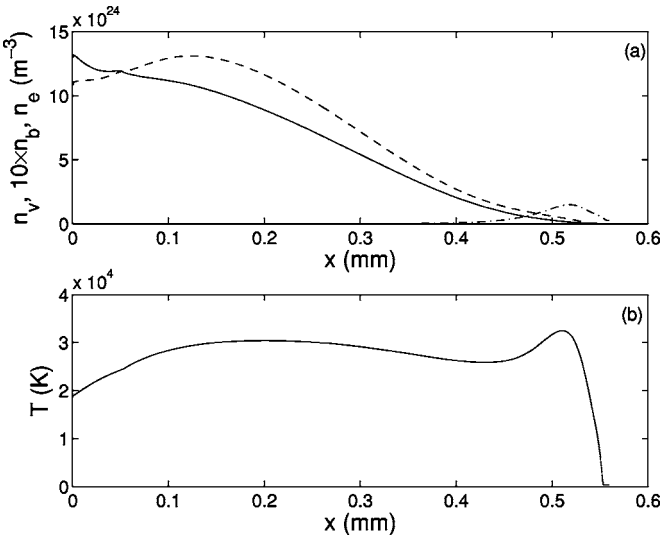

FIG. 9. Spatial distribution of (a) calculated Cu vapor density (solid line), calculated ambient gas density (dash-dotted line), and calculated electron density (dashed line) and (b) calculated plume temperature at 30 ns, for the laser condition shown in Fig. 1 and ambient pressure at 0.01 atm.

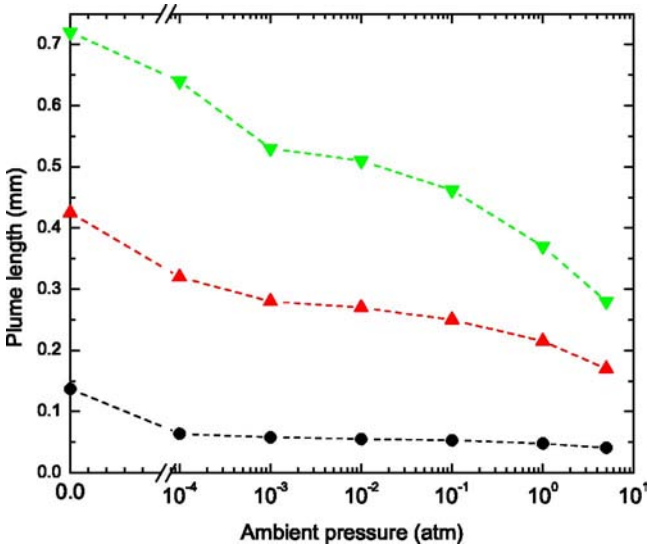

FIG. 10. (Color online) Calculated plume length at different times: 10 (●), 20 (▲), and 30 ns (▼), as a function of ambient pressure, for the condition shown in Fig. 1.

distribution of calculated Cu vapor density, calculated ambient gas density, calculated electron number density, and calculated plume temperature at 30 ns for the case of 1 atm ambient pressure. It is clear that the maximum plume temperature does not locate at the front of the shock wave. Therefore, for high ambient pressures, the maximum plume temperature as it will be plotted in Fig. 11 surely corresponds to the highest temperature in the plume. Moreover, the location of the maximum plume temperature coincides with that of the maximum vapor density. Thus, it is obvious that the locations of the maximum electron density and the maximum vapor density coincide in this case. For the case of lower ambient pressures, the situation changes: the maximum plume temperature may appear at the front of the shock wave. Figure 9 presents the result at 30 ns for the case of 0.01 atm ambient pressure. Notice that the temperature at the shock-wave front cannot reflect the main feature of the plume (or plasma) because the density of the vapor is extremely small there. Therefore, in the following, the definition of the maximum plume temperature always means the highest temperature in the central part of the plume. In this way, it makes sense to have a general definition for the maximum plume temperature at various ambient pressures, which reflects the characteristic of the laser-induced plasma. The maximum vapor density locates near the target surface or in the central part of the plume, depending on the specific ambient pressure and the time. This causes that the location of the maximum electron density is different from that of the maximum vapor density. However, the location of the maximum electron density coincides with that of the maximum temperature in the central part of the plume.

Figure 10 presents the calculated plume length at different times at various ambient pressures. At 10 ns, the plume length for the case of vacuum is already much larger than that for other ambient pressures. Also one can notice that at this time the difference among the plume lengths at different ambient pressures is very small. Looking at the results at 20 and 30 ns, one can find that the plume expansion into vacuum is close to a free expansion. This agrees well with the results obtained in Ref. 35. For the case of other various ambient pressures, it can be seen in Fig. 10 that the plume size at the same time decreases monotonously with increasing the ambient pressures. This reflects the confinement exerted by the background gas. The higher the ambient pressure, the stronger the confinement and the shorter the plume length. For example, at 30 ns, the plume length for 10^{-4} atm is about 0.65 mm, but it is only 0.37 mm for 1 atm.

The calculated maximum plume temperatures at different times for various ambient pressures are shown in Fig. 11. One can see that at 10 ns the maximum plume temperature in the vacuum case is larger than that in other cases. Besides, at 10 ns, the maximum plume temperature for ambient pressure ranging from 0.001 to 5 atm only varies very slightly. When time evolves, the maximum plume temperature drops mo-

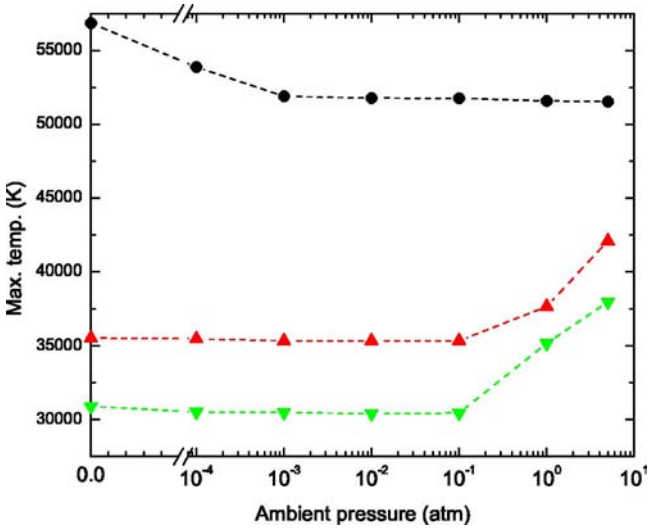

FIG. 11. (Color online) Calculated maximum plume temperature at different times: 10 (●), 20 (▲), and 30 ns (▼), as a function of ambient pressure, for the condition shown in Fig. 1.

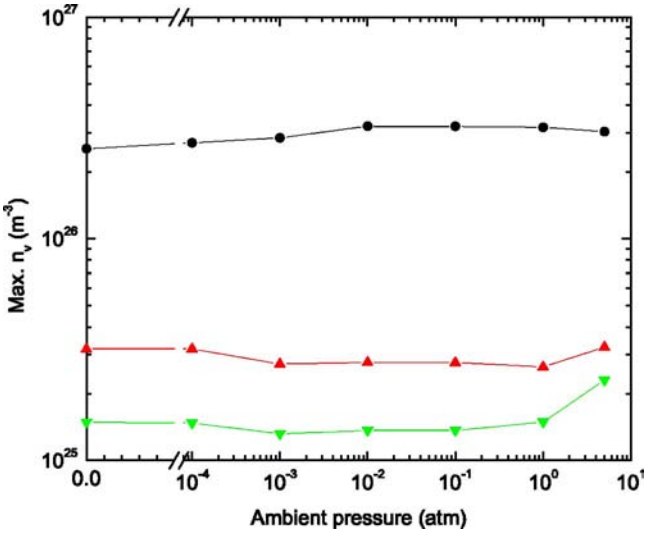

FIG. 12. (Color online) Calculated maximum Cu vapor density at different times: 10 (●), 20 (▲), and 30 ns (▼), as a function of ambient pressure, for the condition shown in Fig. 1.

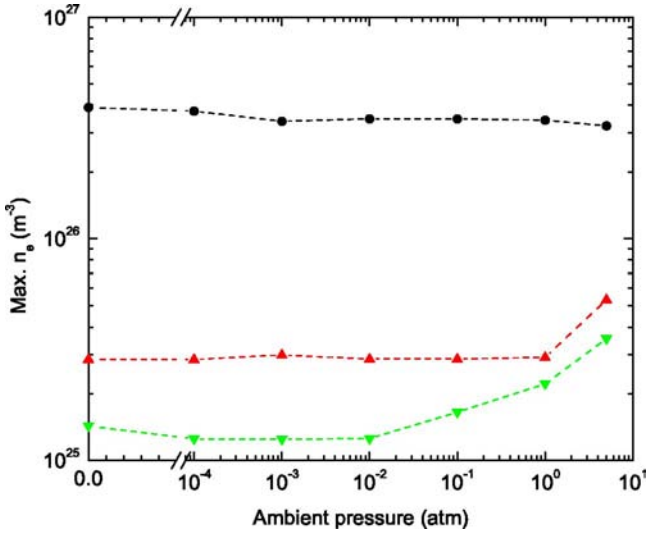

FIG. 13. (Color online) Calculated maximum electron density in the plume at different times: 10 (●), 20 (▲), and 30 ns (▼), as a function of ambient pressure, for the condition shown in Fig. 1.

notonously in all cases. However, when time evolves into 20 or 30 ns, the maximum plume temperature for 1 and 5 atm is obviously higher than that in other cases. It means that the decrease rate of the maximum plume temperature for higher ambient pressures is much smaller than that for lower ambient pressures. In other words, the hot core of the plume (plasma) can last a longer period of time for higher ambient pressures than for lower ambient pressures. On the other hand, at later times, in the ambient range between 0 and 0.1 atm, the maximum plume temperature becomes very similar.

Figure 12 shows the effect of the pressure on the calculated maximum Cu vapor density at different times. At 10 ns, the maximum Cu vapor density has the highest value at ambient pressure of 0.01 atm. However, the maximum Cu vapor densities for all pressures at 10 ns are still very close and in the order of 10^{26} m^{-3}. Along with time, the maximum vapor density starts to decrease monotonously. When the time evolves to 30 ns, the maximum Cu vapor density at 5 atm is significantly larger than at other pressures. This also reflects the confinement effect of the background gas.

The calculated maximum electron densities in the plume at different times for various ambient pressures are presented in Fig. 13. In general, the feature of the maximum electron density is similar to that of the maximum Cu vapor density, because the main source of the electrons comes from the ionization of Cu vapor. However, one can find that at 10 ns, the maximum electron number density in the vacuum case is the highest among all cases. At later times, the highest value of the maximum electron density is observed in the 5 atm case. This exhibits a very complicated effect of ambient pressure on the maximum electron density. However, the complex behavior can be partly inferred from Figs. 8 and 9, which show that the location of the maximum plume temperature and that of the maximum vapor density may be different when the ambient pressures vary.

Looking back to Figs. 10–13, one may conclude that under the applied laser condition, there are several common characteristics of the plume for different ambient pressures: (1) the larger the ambient pressure, the shorter the plume length; (2) the maximum plume temperature is in the order of several 10^4 K; (3) the maximum Cu vapor density for the ambient pressure ranging from 0 to 1 atm has a very similar feature; (4) for the case of ambient pressures lower than 1 atm, the maximum electron density exhibits a similar behavior; and (5) the decrease rate of the maximum Cu vapor density, the maximum plume temperature, and the maximum electron density for higher ambient pressures (e.g., 1 or 5 atm) is much smaller than that for lower ambient pressures.

Finally, in order to validate our calculated results, they need to be compared with experimental data. It is hard to find experimental data in the literature for the plume temperature, the electron density, and other plume/plasma characteristics, at the early stage. In Ref. 32 we have compared our calculated results for a wide range of laser conditions (laser intensities, pulse duration, and wavelength) at ambient gas pressure of 1 atm, with available literature data, and the agreement was quite satisfactory. In the present paper, we perform an indirect comparison between our modeling and ablation experiments recently carried out using a Nd:YAG(yttrium aluminum garnet) laser operated under the following conditions: laser pulse energy of 4 mJ (measured behind a microscope without a focusing lens, to avoid burning the detector), pulse length of 6 ns, repetition rate of 10 Hz, 200 shots delivered, wavelength of 266 nm (Nd:YAG), and spot size of 170 μm. The ambient gas is He at 1 atm pressure. The crater morphology was investigated using surface profilometry. Five traces were acquired of the crater morphology, each 20 μm aside of the previous, and then averaged to get the measured depth profile of the crater. The acquisition was done with a stylus force of 5.0 mg, a moving speed of 20 μm/s, and over a distance of 500 μm across the crater. After calculating the energy, pulse length, and spot size, we estimate that if a Gaussian-shaped laser pulse is applied with 6 ns FWHM, it should have a peak

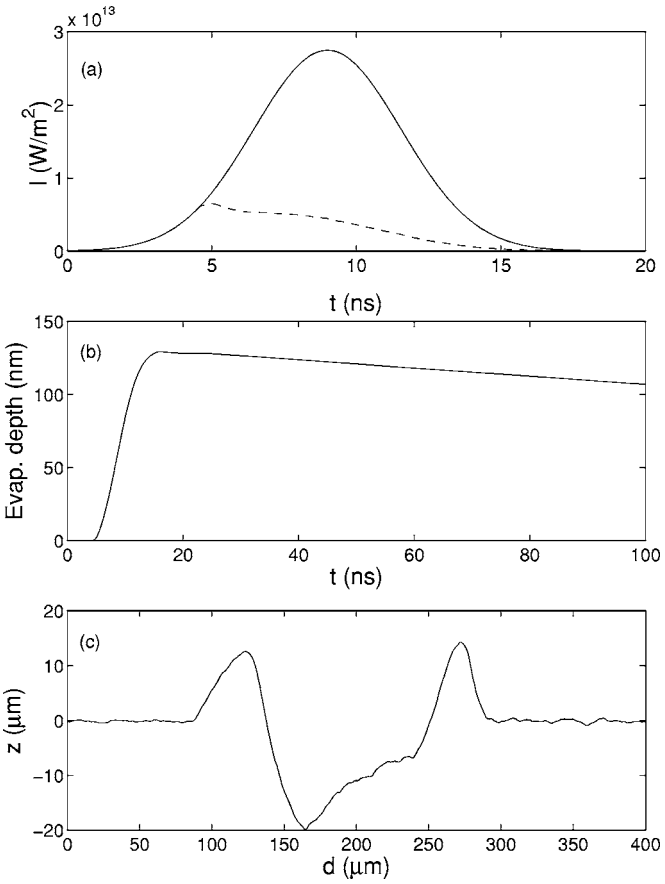

FIG. 14. (a) Laser intensity-time profile. It is a Gaussian-shaped pulse with 6 ns full width at half maximum and peak irradiance of 2.76×10^9 W/cm^2. The solid line represents the original laser pulse and the dashed line represents the calculated laser irradiance arriving at the target, after passing through the plume (plasma). (b) Calculated evaporation depth vs time for the laser condition given in (a). (c) Measured target surface depth profile after 200 laser pulses.

irradiance of 2.76×10^9 W/cm^2. Figure 14 shows the calculated results and the experimental result. In Fig. 14(a), the original laser pulse shape and the calculated laser irradiance after plasma shielding are given. Notice that the laser energy absorbed by the plasma is as high as 75% of that of the original laser pulse. Figure 14(b) shows the calculated evaporation depth as a function of time. Since the recondensation was taken into account in our model, after the laser pulse is finished the evaporation depth will decrease gradually. At 20 ns, the evaporation depth is around 130 nm; however, at 100 ns, the evaporation depth is about 107 nm. Figure 14(c) presents the averaged measurements of the target depth profile after 200 shots. The crater floor was not at all flat which might be due to the fact that the beam energy profile is not homogenized. However, to check if the vaporization process is mainly responsible for the material removal at the laser conditions discussed in the paper, one can compare the measured depth of the crater and the calculated value based on the vaporization process considered in the paper. When looking at the measured depth of the crater shown in Fig. 14(c), it turns out that for one shot (or single pulse) the evaporation depth is around $1/200\times20$ μm $=100$ nm. Comparing the calculated evaporation depth of 107 nm [shown in Fig. 14(b)] and the measured value of 100 nm, one may conclude that the model prediction agrees very well with the experiment. This agreement indirectly confirms the validity of the modeling work, because at a peak irradiance as high as 2.76×10^9 W/cm^2 the accurate calculation of the plume characteristics is crucial to give a correct prediction of the plasma shielding, which determines the target surface temperature, and hence also the evaporation depth. One may notice from Fig. 14(c) that the trace around the crater is not completely flat; this may be due to the presence of falloff particulate of a few microns in size at the margins of the crater in the experiments. Furthermore, the edges of the crater are characterized by a pronounced upheaval produced by hydrodynamic instability of the molten material. The elevation is proportional to the melt lifetime and pressure field induced by the pulse in the melt pool. The presence of a significant crater wall is typical for metallic targets irradiated.[40] It should be pointed out that the presence of the nonflat trace and the elevation of the crater edge in the experiments are not due to the vaporization process and cannot be simulated with our current model. We plan to develop a model to include the mechanisms responsible for these phenomena in the near future.

IV. CONCLUSION

A comprehensive numerical model for nanosecond-LA of metallic targets, based on target heating, melting and vaporization, plume expansion in 1 atm background gas, plasma formation, and laser absorption in the plasma, was recently developed[31] and is applied here to investigate the effect of ambient pressure on the target and the plume/plasma expansion under a fixed laser condition. Since the laser pulse applied in the paper has a fluence much higher than the threshold for the plasma formation in the plume,[32] there is always a plasma formed in the plume expansion at the early stage, regardless of the ambient pressure. The effect of ambient pressure shows that generally the characteristic of the heating, melting and vaporization of the target at various ambient pressures is very similar. With the applied laser pulse, the maximum surface temperature decreases slightly by less than 300 K when the ambient pressure varies from 0 to 5 atm. Also, the maximum evaporation rate and the evaporation depth at various ambient pressure are very similar. The fraction of laser energy absorbed by the plume only differs less than 3% for different ambient pressures. However, the plume lengths at different ambient pressures are quite different: the larger the ambient pressure, the shorter the plume length. For the same laser pulse, the maximum plume temperature at various ambient pressures is in the same order of a few 10^4 K. But at higher ambient pressures, the maximum plume temperature decreases more slowly. Meanwhile, at later times, the maximum vapor density and the maximum electron density drop more slowly at higher ambient pressures than at lower ambient pressures.

The experimental determination of the plasma characteristics during the early times of laser ablation and plume expansion appears to be difficult, because of the high optical thickness of the spectral lines emitted from the initial dense plasma. However, we have compared our calculated evapo-

ration depth at a high laser fluence with an experiment on the ablation of Cu in 1 atm He gas. It is found that the calculated result is in good agreement with the measurement. This indicates how valuable such modeling calculations can be, because they can give insight in the plume dynamics and plasma behavior, which is sometimes difficult to obtain from experiments.

This model was primarily developed to describe LA for chemical analysis applications, such as LIBS and as a sample introduction method for ICPs, where the background gas is generally at 1 atm. However, to apply the model also to other applications, such as PLD, where the background gas is at low pressure, we have carried out an investigation for the effect of ambient gas pressure, from vacuum till above 1 atm (i.e., 5 atm). The model results are very useful for obtaining more fundamental insight in the effect of a background gas. The model works from the stage of a plume without any ionization to that of a fully ionized plasma. This suggests that there may be some other applications in laser ablation where the ionization process needs to be considered. As we have discussed in the Introduction section, for different ambient pressures, the plume expansion into radial direction becomes important at different times. It is necessary to extend the model to two dimensions for the later stages of plume expansion.

ACKNOWLEDGMENTS

One of the authors (Z.C.) is financed by a bilateral project between Flanders and China. The authors thank A. Vertes for supplying the original code for laser ablation in vacuum and A. Vertes and R. Gijbels for the interesting discussions. Swiss Federal Laboratory for Material Testing (EMPA) is acknowledged for the laser ablation facility, which was redesigned and run by one of the authors (D.B.). Olga Guseva (EMPA) is acknowledged for assistance during the profilometry measurement. Christian Bottali and Francisco Alvarez (EMPA) are acknowledged for preparation of the metallic targets.

[1]M. Von Allmen, *Laser Beam Interactions with Materials* (Springer, Heidelberg, 1987).
[2]D. B. Chrisey and G. K. Hubler, *Pulsed Laser Deposition of Thin Films* (Wiley, New York, 1994).
[3]A. G. Gnedovets, A. V. Gusarov, and I. Smurov, J. Phys. D **32**, 2162 (1999).
[4]S. S. Harilal, C. V. Bindhu, M. S. Tillack, F. Najmabadi, and A. C. Gaeris, J. Appl. Phys. **93**, 2380 (2003).
[5]H. W. Kroto, J. R. Heath, S. C. O'Brien, R. F. Curl, and R. E. Smalley, Nature (London) **318**, 162 (1985).
[6]L. J. Radziemski, Spectrochim. Acta, Part B **57**, 1109 (2002).
[7]R. E. Russo, Appl. Spectrosc. **49**, 14A (1995).
[8]D. Günther, S. E. Jackson, and H. P. Longerich, Spectrochim. Acta, Part B **54**, 381 (1999).
[9]R. E. Russo, X. Mao, and S. S. Mao, Anal. Chem. **74**, 70A (2002).
[10]Yu. I. Koptev, *Gas Dynamics* (Nova Science, New York, 1992).
[11]V. Detalle, M. Sabsabi, L. St-Onge, A. Hamel, and R. Héon, Appl. Opt. **42**, 5971 (2003).
[12]I. NoorBatcha, R. R. Lucchese, and Y. Zeiri, J. Chem. Phys. **86**, 5816 (1987).
[13]D. Sibold and H. M. Urbassek, J. Appl. Phys. **73**, 8544 (1993).
[14]T. E. Itina, V. N. Tokarev, W. Marine, and M. Autric, J. Chem. Phys. **106**, 8905 (1997).
[15]F. Garrelie, J. Aubreton, and A. Catherinot, J. Appl. Phys. **83**, 5075 (1998).
[16]J. C. S. Kools, J. Appl. Phys. **74**, 6401 (1993).
[17]M. Aden, E. Beyer, G. Herziger, and H. Kunze, J. Phys. D **25**, 57 (1992).
[18]M. Aden, E. W. Kreutz, and A. Voss, J. Phys. D **26**, 1545 (1993).
[19]J. R. Ho, C. P. Grigoropoulos, and J. A. C. Humphrey, J. Appl. Phys. **78**, 4696 (1995).
[20]J. R. Ho, C. P. Grigoropoulos, and J. A. C. Humphrey, J. Appl. Phys. **79**, 7205 (1996).
[21]C. L. Liu, J. N. Leboeuf, R. F. Wood, D. B. Geobegan, J. M. Donato, K. R. Chen, and A. A. Puretzky, Mater. Sci. Eng., B **47**, 70 (1997).
[22]R. F. Wood, K. R. Chen, J. N. Leboeuf, A. A. Puretzky, and D. B. Geohegan, Phys. Rev. Lett. **79**, 1571 (1997).
[23]A. V. Bulgakov and N. M. Bulgakova, J. Phys. D **28**, 1710 (1995).
[24]A. V. Gusarov and A. G. Gnedeovets, J. Appl. Phys. **88**, 4352 (2000).
[25]Z. Y. Zhang, Z. Y. Han, and G. S. Dulikravich, J. Appl. Phys. **90**, 5889 (2001).
[26]A. V. Gusarov and I. Smurov, J. Phys. D **36**, 2962 (2003).
[27]M. Capitelli, A. Casavola, G. Golonna, and A. De Giacomo, Spectrochim. Acta, Part B **59**, 271 (2004).
[28]T. E. Itina, J. Hermann, Ph. Delaporte, and M. Sentis, Phys. Rev. E **66**, 066406 (2002).
[29]T. E. Itina, J. Hermann, Ph. Delaporte, and M. Sentis, Appl. Surf. Sci. **208–209**, 27 (2003).
[30]H. C. Le, D. E. Zeitoun, J. D. Parisse, M. Sentis, and W. Marine, Phys. Rev. E **62**, 4152 (2000).
[31]Z. Y. Chen and A. Bogaerts, J. Appl. Phys. **97**, 063305 (2005).
[32]A. Bogaerts and Z. Y. Chen, Spectrochim. Acta, Part B **60**, 1280 (2005).
[33]K. R. Chen, J. N. Leboeuf, R. F. Wood, D. B. Geohegan, J. M. Donato, C. L. Liu, and A. A. Puretzky, Appl. Surf. Sci. **96–98**, 14 (1996).
[34]A. K. Sharma and R. K. Thareja, Appl. Surf. Sci. **243**, 68 (2005).
[35]A. Bogaerts, Z. Y. Chen, R. Gijbels, and A. Vertes, Spectrochim. Acta, Part B **58**, 1867 (2003).
[36]L. Balazs, R. Gijbels, and A. Vertes, Anal. Chem. **63**, 314 (1991).
[37]H. Schittenhelm, G. Callies, P. Berger, and H. Hugel, J. Phys. D **29**, 1564 (1996).
[38]X. Zhang, S. S. Chu, J. R. Ho, and C. P. Grigoropoulos, Appl. Phys. A: Mater. Sci. Process. **A64**, 545 (1997).
[39]G. Callies, P. Berger, and H. Huëgel, J. Phys. D **28**, 794 (1995).
[40]D. Bleiner, Spectrochim. Acta, Part B **60**, 49 (2005).